*Technical Note*

# Blind Adaptive Beamforming for a Global Navigation Satellite System Array Receiver Based on Direction Lock Loop

**Jian Wu, Xiaomei Tang \*, Long Huang, Shaojie Ni and Feixue Wang**

College of Electronic Science and Technology, National University of Defense Technology, Changsha 410073, China; wujian@nudt.edu.cn (J.W.); longhuang@nudt.edu.cn (L.H.); nishaojie@nudt.edu.cn (S.N.); wangfeixue_nnc@163.com (F.W.)
\* Correspondence: txm_nnc@126.com

**Abstract:** The adaptive beamforming algorithm can realize interference suppression and navigation signal enhancement, and has been widely used. However, achieving high-precision real-time estimation of the direction of arrival (DOA) parameters of navigation signals in strong-interference scenarios with low complexity is still a challenge. In this paper, a blind adaptive beamforming algorithm for a Global Navigation Satellite System (GNSS) array receiver based on direction lock loop is proposed without using the prior information of the DOA parameter. The direction lock loop is used for DOA tracking and estimation after interference suppression, which uses the spatial correlation of the array beam pattern to construct a closed direction-tracking loop. The DOA estimation value is adjusted in real time based on the loop errors. A blind beamformer is constructed using the DOA estimation results to provide gain by forming a beam in the satellite direction. This method improves the accuracy and dynamic adaptability of DOA estimation while significantly reducing the computational complexity. The theoretical analysis and simulation results verify the effectiveness of the proposed algorithm.

**Keywords:** GNSS; blind adaptive beamforming; direction lock loop; array antenna; DOA estimation

## 1. Introduction

The Global Navigation Satellite System (GNSS) can provide high-precision positioning, navigation and timing services [1]. However, the satellite navigation signal is very weak and buried in noise, which is easily affected by intentional and unintentional interference [2–4]. The array anti-jamming method can improve the interference suppression capabilities by using an adaptive antenna array, and has become one of the most useful anti-jamming methods [5,6].

The blind interference suppression algorithms, such as the power inversion (PI) algorithm [7,8], can suppress the interference without using the prior knowledge of the direction of arrival (DOA) parameter of the satellite signal. However, these methods are unable to enhance the navigation signal energy, and may even reduce the signal-to-noise ratio [9].

The beamforming method [10] forms a null in the direction of the interference and points the beam in the direction of the navigation signal, thereby achieving interference suppression while increasing the energy of the useful signal, which can effectively improve the weak signal reception capability. The Minimum Variance Distortionless Response (MVDR) method [11] is the most commonly used beamforming method, which uses the prior DOA information of the incident signal to construct the beamformer. This method generally needs to obtain the real-time attitude information of the array antenna by means of inertial navigation; however, most array antennas cannot provide this.

Blind beamforming algorithms can achieve similar effects to MVDR by using the DOA estimation method without prior information [12,13]. The DOA parameters of the incident signal are estimated in real time by the array signal processing method. The

attitude information of the array antenna is not required as a priori information. The commonly used DOA parameter estimation methods include subspace-based methods such as MUSIC [14] and ESPRIT [15], the maximum likelihood estimator (MLE) method [16], the parse recovery method [17], etc. However, the DOA estimation performance of these methods in dynamic scenes will decrease because the target motion will degrade the spectral resolution of the array [18]. At the same time, the computational complexity of these methods is high, which is not applicable for the actual navigation receiver.

Direction lock loop (DiLL) [19–21] can achieve high-precision DOA parameter tracking, which is very suitable for a direct sequence code division multiple access (DS-CDMA) system. DiLL uses the left-shifted and right-shifted spatial array response vectors to construct a closed loop for direction tracking, which can reduce the computational complexity significantly [22].

In Ref. [23], DiLL is used for the DOA estimation of mobile target, which can achieve a high-resolution DOA estimate signal. In Ref. [24], a DOA tracking method based on DiLL with tracking bias compensation for GNSS receivers was proposed, in which the tracking bias was effectively eliminated by estimating and compensating the error in real time. In Ref. [22], the rotate-to-zero DiLL (RZ-DiLL) method was proposed, which could effectively improve the DOA parameter estimation accuracy of large-angle incident signals. In Ref. [25], a DiLL method for a three-element L-shaped array was proposed to achieve the fast acquisition and tracking of two-dimensional DOA parameters, which significantly simplified the antenna structure and eliminated the dead-zone effect. However, most of the above methods are only suitable for non-interference scenarios. The realization of DOA tracking in strong interference scenarios is in urgent need of research.

In this paper, a blind beamforming method for a GNSS array receiver based on DiLL is proposed. Firstly, the subspace projection method is used to suppress the interference signal. Secondly, the DOA parameter of the navigation signal is tracked and estimated by using the DiLL method after interference suppression. Thirdly, the estimated DOA parameters are used to construct the beamformer, which can achieve interference suppression and signal enhancement. The contribution and novelty are reflected in the following aspects:

1.　The DOA parameter of the GNSS signal can be estimated accurately in strong interference scenarios. It solves the problem that it is difficult to achieve both interference suppression and DOA estimation with traditional methods.
2.　The proposed method can realize DOA parameter estimation with low computational complexity, and thus stable DOA tracking in dynamic scenes. It is very suitable for the GNSS receiver, which needs real-time processing.
3.　The blind adaptive beamformer is constructed using the estimated DOA parameter, which can realize interference suppression and navigation signal enhancement. It can achieve almost the same performance as the MVDR method.

The remainder of this paper is organized as follows: Section 2 presents the signal model. Section 3 presents the proposed blind adaptive beamforming method based on DiLL. Section 4 gives the simulation results, and Section 5 concludes this paper.

## 2. Signal Model

In order to simplify the analysis without loss of generality, under the far-field condition, it is assumed that a single navigation signal and $Q$ interference signal occur on the uniform line array (ULA) simultaneously. The ULA has $N$ antenna elements. The array configuration of the ULA is shown in Figure 1.
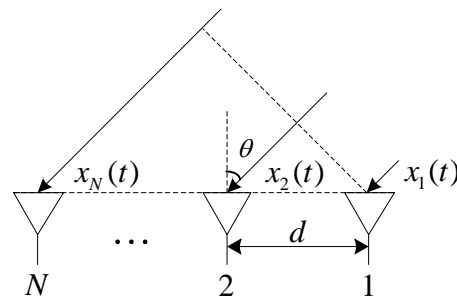
**Figure 1.** Array configuration of the ULA.

The coupled signal received by the GNSS receiver can be expressed as

$$\mathbf{x}(t) = \mathbf{a}(\theta_0)s(t - \tau_0) + \sum_{q=1}^{Q} \mathbf{a}(\theta_q)j_q(t) + \mathbf{n}(t) \tag{1}$$

where $\mathbf{x}(t) = [x_1(t), x_2(t), \cdots, x_N(t)]^T$ stands for array data vector. $s(t)$ represents the baseband GNSS signal, $\tau_0$ and $\theta_0$ are the time delay and DOA parameter of GNSS signal, respectively. $j_q$ denotes the $q$th interference signal component with DOA parameter $\theta_q$. $\mathbf{n}(t)$ represents the additive white Gaussian noise vector, and $\mathbf{a}(\theta)$ is the array guide vector, which can be expressed as

$$\mathbf{a}(\theta) = \left[ 1, e^{-j2\pi d \sin(\theta)/\lambda}, \cdots, e^{-j2\pi d(N-1)\sin(\theta)/\lambda} \right]^T \tag{2}$$

where $\theta$ is the signal incident angle, $\lambda$ is the wavelength, and $d = \lambda/2$ is the array spacing.

The baseband GNSS signal $s(t - \tau_0)$ can be expressed as

$$s(t - \tau_0) = A \cdot D(t - \tau_0)c(t - \tau_0)e^{j(2\pi f_d t + \varphi)} \tag{3}$$

where $D(\cdot)$ indicates the message bit. In this paper, the correlation accumulation time is all within a bit range, so the navigation message is assumed to be constant, i.e., 1. $c(\cdot)$ represents a pseudo-random noise (PRN) code. $A$, $f_d$, and $\varphi$ represent navigation signal amplitude, Doppler frequency, and carrier phase, respectively.

By constructing an array beamformer, the array can be weighted to achieve an effective suppression of interference. The output after array weighting is

$$
\begin{aligned}
y(t) &= \mathbf{w}^H \mathbf{x} \\
&= \mathbf{w}^H \mathbf{a}(\theta_0)s(t - \tau_0) + \sum_{q=1}^{Q} \mathbf{w}^H \mathbf{a}(\theta_q)j_q(t) + \mathbf{w}^H \mathbf{n}(t) \\
&\approx \mathbf{w}^H \mathbf{a}(\theta_0)s(t - \tau_0) + \mathbf{w}^H \mathbf{n}(t)
\end{aligned} \tag{4}
$$

where $\mathbf{w}$ stands for array weight vector.

## 3. Blind Adaptive Beamforming Based on Direction Lock Loop

### 3.1. Interference Suppression

Since the power of the interference signal is much higher than that of the navigation signal, the covariance matrix of the array signal is determined mainly by the interference and noise terms.

$$\mathbf{R} = E\left[ \mathbf{x}\mathbf{x}^H \right] = \sum_{n=1}^{N} \lambda_n \mathbf{u}_n \mathbf{u}_n^H = \sum_{n=1}^{Q} (\lambda_n - \sigma_e^2)\mathbf{u}_n \mathbf{u}_n^H + \sigma_e^2 \mathbf{I}_{N \times N} \tag{5}$$

where $\lambda_n$ and $\mathbf{u}_n(n = 1, 2, \cdots, N)$ denote the eigenvalues and the corresponding eigenvectors of $\mathbf{R}$. $\sigma_e^2$ represents the power of the noise. The eigenvalues are arranged in descending order:

$$\lambda_1 \geq \lambda_2 \geq \cdots \geq \lambda_Q \gg \lambda_{Q+1} = \cdots = \lambda_N = \sigma_e^2 \tag{6}$$

The inverse matrix $\mathbf{R}^{-1}$ can be calculated as

$$
\begin{aligned}
\mathbf{R}^{-1} &= \sum_{n=1}^{N} \frac{1}{\lambda_n} \mathbf{u}_n \mathbf{u}_n^H \\
&= \sum_{n=1}^{Q} \frac{1}{\lambda_n} \mathbf{u}_n \mathbf{u}_n^H + \frac{1}{\sigma_e^2} \sum_{n=Q+1}^{N} \mathbf{u}_n \mathbf{u}_n^H \\
&= \frac{1}{\sigma_e^2} \left( \mathbf{I}_{N \times N} - \sum_{n=1}^{Q} \frac{\lambda_n - \sigma_e^2}{\lambda_n} \mathbf{u}_n \mathbf{u}_n^H \right)
\end{aligned}
\tag{7}
$$

Assuming the interference power is much larger than the noise power, the orthogonal complementary space $\mathbf{U}_I^{\perp}$ can be approximated by the inverse of the covariance matrix $\mathbf{R}$ [26], i.e.,

$$\mathbf{R}^{-1} \approx \frac{1}{\sigma_e^2} \mathbf{U}_I^{\perp} \tag{8}$$

In Equation (8), the coefficient $1/\sigma_e^2$ is a constant related to the noise power, which can be omitted. There is no need to perform eigenvalue decomposition, which can significantly reduce the amount of computation. By projecting the array signal into the orthogonal complementary space, the interference can be mitigated. The array signal after the interference suppression can be expressed as

$$\hat{\mathbf{x}}(t) \approx \mathbf{R}^{-1} \mathbf{x} \tag{9}$$

### 3.2. DOA Tracking Based on DiLL

Since the navigation signal is very weak and buried under the noise, the correlation accumulation with the locally copied pseudo-code signal is required to improve the signal-to-noise ratio. The correlation results can be modeled as

$$\mathbf{r} = E[\hat{\mathbf{x}}(t) \cdot c_L^*(t - \hat{\tau})] = \mathbf{R}^{-1} \mathbf{a}(\theta_0) r_0(\Delta\tau) \tag{10}$$

where $r_0(\Delta\tau)$ represents the correlation summation value between the received navigation signal and the local replica pseudo-code. $c_L(t - \hat{\tau})$ is the local replica PRN code, and $\Delta\tau = \tau_0 - \hat{\tau}$ represents the estimation error of the time delay. The carrier is considered to be completely wiped off.

From Equation (10), it can be seen that the correlation accumulation vector is closely related to the incident angle of the received signal. The array direction diagram is constructed by using this vector as the weight vector. Then, the gain is maximum in the direction of the signal incident.

The normalized array pattern of the ULA is shown in Figure 2. The normalized spatial correlation function can be defined as

$$R(\theta, \theta + \Delta\theta) = \frac{1}{N} \mathbf{a}^H(\theta + \Delta\theta) \mathbf{a}(\theta) = \frac{1}{N} \sum_{n=1}^{N} e^{-j\pi(n-1)(\sin\theta - \sin(\theta + \Delta\theta))} \tag{11}$$

where $(\cdot)^H$ denotes the Hermitian transform and $\Delta\theta$ is the direction bias.
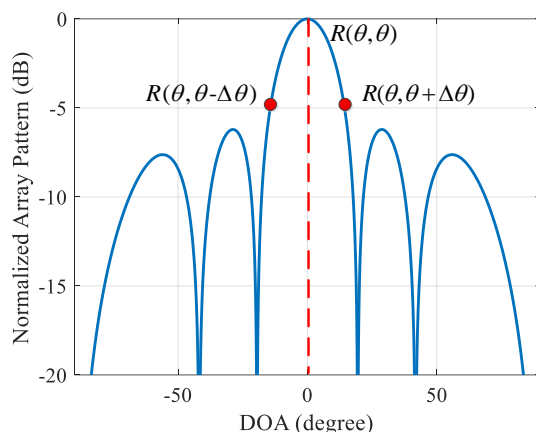
**Figure 2.** Normalized array pattern of the ULA.

The array pattern is symmetrical around the central direction, so

$$R(\theta, \theta + \Delta\theta) \approx R(\theta, \theta - \Delta\theta) \tag{12}$$

The direction can be tracked as the same principle of the code DLL loop. Assuming that the estimated value of DOA at time $k$ is $\hat{\theta}_k$, the array guide vectors $\mathbf{a}(\hat{\theta}_k - \Delta\theta)$ and $\mathbf{a}(\hat{\theta}_k + \Delta\theta)$ of the left and right offset $\Delta\theta$ of the current observed DOA are constructed. After correlating with the estimated signal vector, the spatial correlation functions can be obtained as

$$z_R(k) = \frac{1}{N}\mathbf{a}^H(\hat{\theta}_k + \Delta\theta)\mathbf{r} = \frac{1}{N}r_0(\Delta\tau)\mathbf{a}^H(\hat{\theta}_k + \Delta\theta)\mathbf{R}^{-1}\mathbf{a}(\theta_0) = r_0(\Delta\tau)R'(\theta_0, \hat{\theta}_k + \Delta\theta) \tag{13}$$

$$z_L(k) = \frac{1}{N}\mathbf{a}^H(\hat{\theta}_k - \Delta\theta)\mathbf{r} = \frac{1}{N}r_0(\Delta\tau)\mathbf{a}^H(\hat{\theta}_k - \Delta\theta)\mathbf{R}^{-1}\mathbf{a}(\theta_0) = r_0(\Delta\tau)R'(\theta_0, \hat{\theta}_k - \Delta\theta) \tag{14}$$

where $R'(\theta_1, \theta_2) = \mathbf{a}^H(\theta_2)\mathbf{R}^{-1}\mathbf{a}(\theta_1)/N$ represents the normalized spatial correlation function after interference suppression.

The discrimination error can be expressed as

$$\varepsilon(k) = f[z_R(k), z_L(k)] \tag{15}$$

where $f(\cdot)$ denotes the discriminator function. The coherent DiLL and non-coherent DiLL are the two mainly used direction discriminating functions, which can be expressed as

$$f_{coh}[R_1, R_1] = \text{Re}[R_1 - R_2] \tag{16}$$

$$f_{noncoh}[R_1, R_2] = \frac{|R_1|^2 - |R_2|^2}{|R_1|^2 + |R_2|^2} \tag{17}$$

The S-curves of the coherent DiLL and non-coherent DiLL are shown in Figure 3, in which $N = 4$, $\Delta\theta = 5°$ and $\theta = 0°$. As can be seen from Figure 3, the differential curve shows an approximate linear change near 0 degrees, so the DOA estimation error can be corrected by the discriminator. It also shown that the convergence of the non-coherent DiLL is larger than that of the coherent DiLL.

After loop filtering, the direction discrimination error is sent to the beamforming device to update the DOA parameter value at the next time. Then, the estimated DOA value at time $k + 1$ is

$$\hat{\theta}_{k+1} = \hat{\theta}_k + K_0\varepsilon(k) \otimes h(k) \tag{18}$$

where $h(k)$ stands for loop filter, $\otimes$ represents a convolution operation. If $\hat{\theta}_k < \theta$, then $\varepsilon(k) > 0$, and the estimated value of DOA at the next time will increase; otherwise, the

DOA parameter at the next time will decrease. The accurate estimation of DOA parameters can be achieved through continuous iteration.
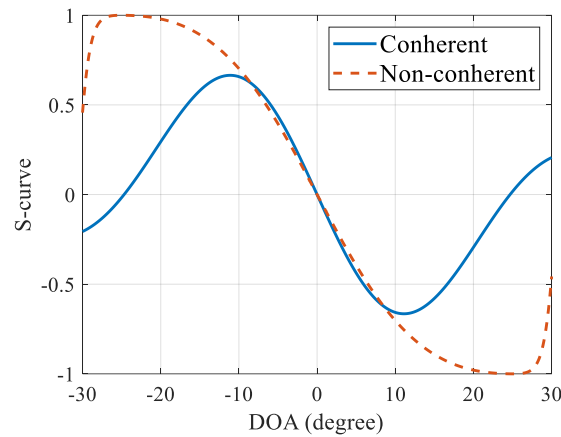


**Figure 3.** The S-curves of the coherent and non-coherent DiLL.

### 3.3. Beamformer Construction

The array vector $\mathbf{a}(\hat{\theta}_k)$ of the signal direction is constructed according to the DOA parameter estimated by DiLL in real time. The output power of the array is minimized, while the response of the signal direction is guaranteed with the unit array:

$$\min_{\mathbf{w}} \left\{ \mathbf{w}^H \mathbf{R} \mathbf{w} \right\} \ s.t. \ \mathbf{w}^H \mathbf{a}(\hat{\theta}_k) = 1 \tag{19}$$

Using the linear constraint minimum variance (LCMV) method to solve the above equation, the optimal weight can be obtained as

$$\mathbf{w}_{opt} = \frac{\mathbf{R}^{-1}\mathbf{a}(\hat{\theta}_k)}{\mathbf{a}^H(\hat{\theta}_k)\mathbf{R}^{-1}\mathbf{a}(\hat{\theta}_k)} \tag{20}$$

The array-weighted output can be calculated as

$$y_{out}(t) = \mathbf{w}_{opt}^H \mathbf{x} \tag{21}$$

### 3.4. The Procedure of the Proposed Method

The diagram of the proposed algorithm is shown in Figure 4 with the following steps.
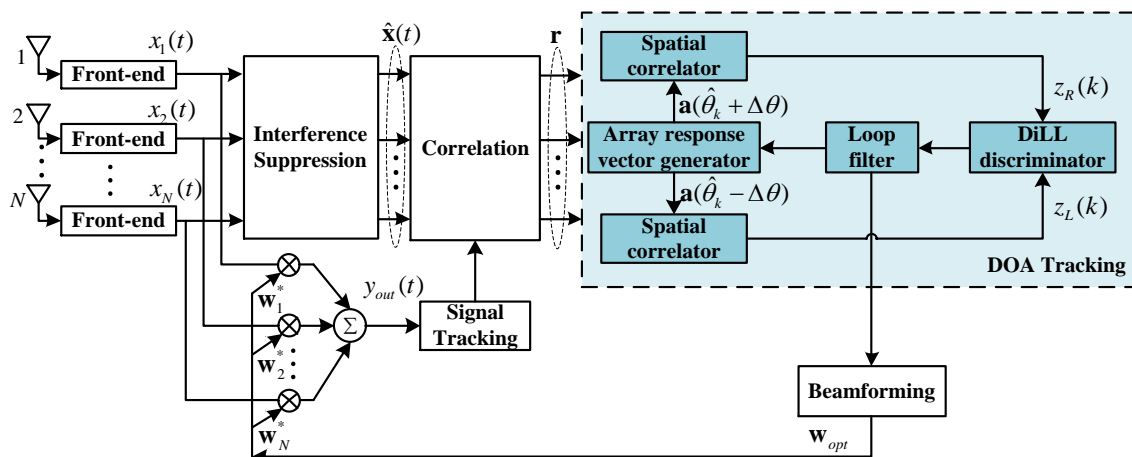


**Figure 4.** Block diagram of the proposed method, $(\cdot)^*$ denotes complex conjugation.

(1) The inverse matrix of the covariance matrix of the array signal was solved and multiplied by the array signal to achieve interference suppression.

(2) The array signal after interference suppression was correlated with the local copied pseudo-code signal to obtain the correlation accumulation vector.

(3) The DiLL method was used to realize the stable tracking processing of the DOA parameters of navigation signals. The spatial correlation values corresponding to the $\Delta\theta$ bias besides the current DOA estimation were constructed, and the revised DOA estimate was obtained after processing and filtering by the discriminator.

(4) The beamformer was constructed according to the estimated DOA value, the array was weighted, and the weighted output signal was used for follow-up tracking processing.

## 4. Simulation Results

### 4.1. DOA Tracking Performance Analysis

The tracking accuracy of DOA is generally characterized by mean square error (MSE), which can be defined as

$$\text{MSE} = \frac{1}{I}\sum_{i=1}^{I}\left(\theta(i) - \hat{\theta}(i)\right)^2 \tag{22}$$

where $\theta(i)$ and $\hat{\theta}(i)$ are the real DOA value and estimation value at the $i$th time, $I$ is the number of processing times.

In this section, the performance of the DOA estimation is evaluated by Monte Carlo simulation. The Monte Carlo simulation was performed 1000 times; $\theta = 0°$ and $\Delta\theta = 5°$. Figure 5 shows the MSE results of the DOA estimation under different carrier-to-noise ratios ($C/N_0$) and different array elements. The performances of the coherent DiLL method, non-coherent DiLL method, and MUSIC method are compared and analyzed. As can be seen from Figure 5, the accuracy of DOA estimation is higher with the increase in the $C/N_0$. Under the same $C/N_0$ condition, the more array elements there are, the higher the estimation accuracy. When the number of array elements is small, the DiLL algorithm can achieve better performance than MUSIC, mainly because when the number of array elements is small, the resolution of the MUSIC algorithm is significantly reduced, while the loop tracking method can still achieve high-precision tracking results. With the increase in the number of array elements, the performance of the MUSIC algorithm is improved and the DiLL algorithm is also effectively improved. Therefore, when the number of array elements is small, the DiLL algorithm has better advantages. It can also be seen that the performance of the coherent DiLL method is better than that of the non-coherent DiLL algorithm.
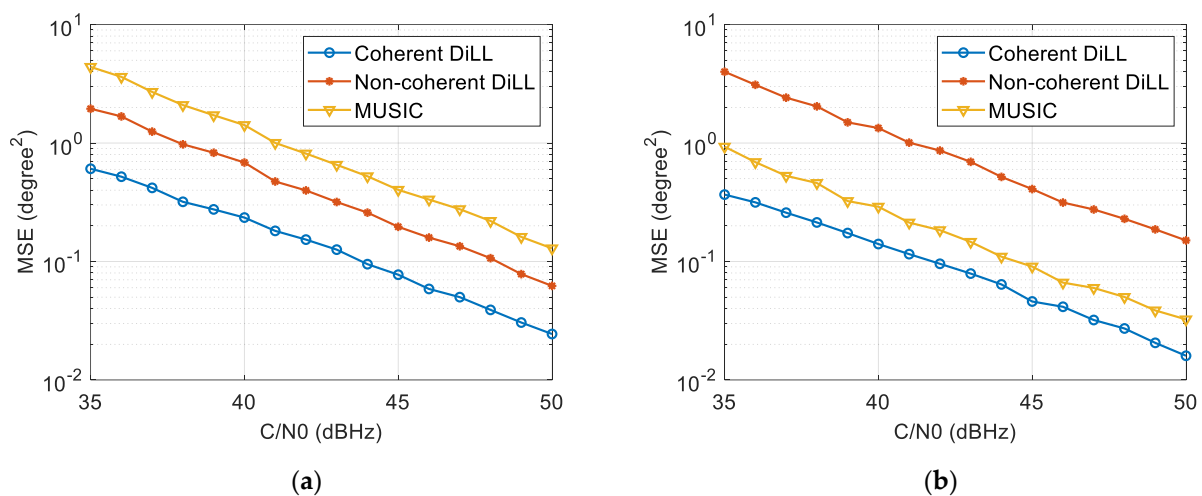


**Figure 5.** MSE estimation results of DOA under different carrier-to-noise ratios: (**a**) DOA estimation results under 6 array elements; (**b**) DOA estimation results under 10 array elements.

### 4.2. Dynamic Adaptability Analysis

　　Through estimating the tracking error and the error compensation, DiLL realizes DOA estimation in real time, and thus stable DOA tracking in dynamic scenes. Typical DOA dynamic change scenarios include fixed DOA parameters, uniform acceleration change, sinusoidal change, and step change. Figures 6–9 give the DiLL tracking performance in these scenarios, respectively. In the simulation, the angle interval is 5 degrees, the number of array elements is eight, and the carrier-to-noise ratio parameter is 40 dBHz.
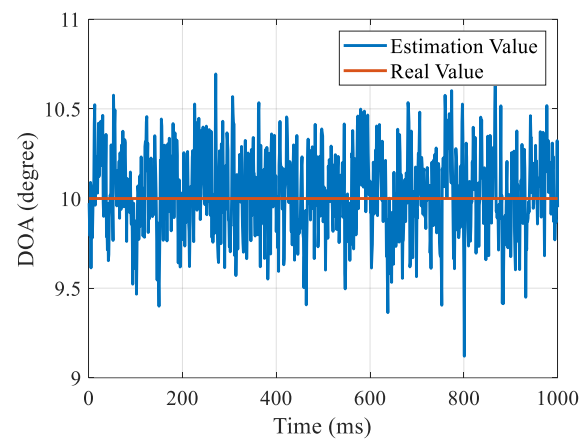


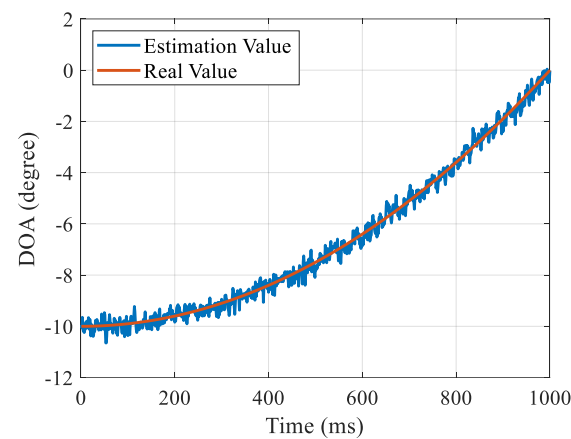**Figure 6.** Tracking results under the scenario of fixed DOA parameters.



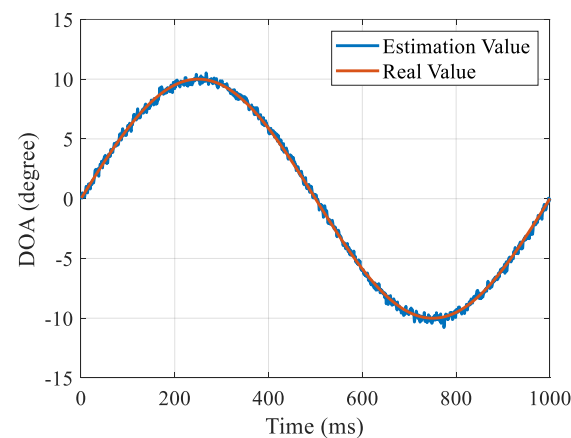**Figure 7.** Tracking results of DOA parameters in uniformly accelerated changing scenarios.



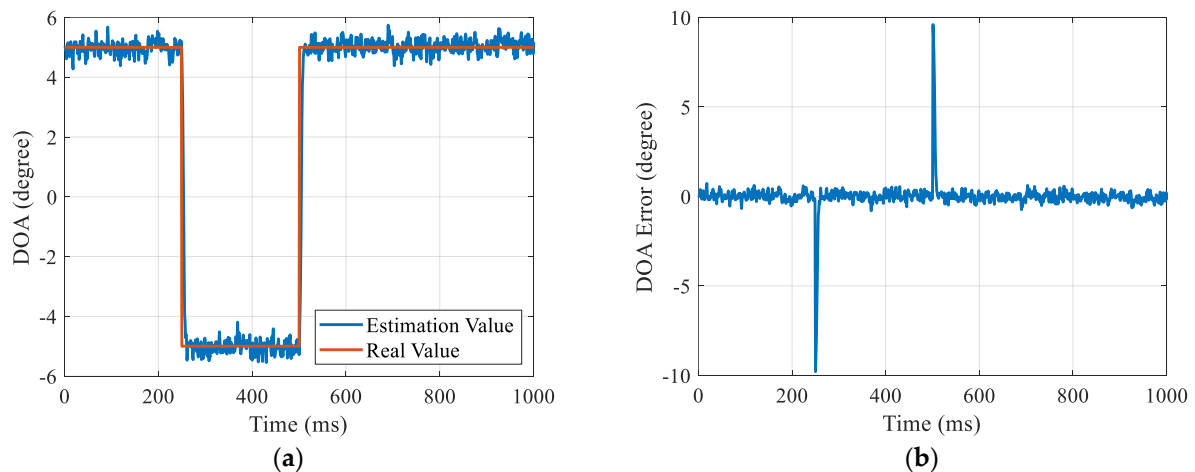**Figure 8.** Tracking results in the scenario of sinusoidal variation in DOA parameters.

**Figure 9.** Tracking results in the scenario of DOA parameter step change: (**a**) DOA tracking results; (**b**) DOA tracking error.

Figure 6 shows the tracking results under fixed DOA conditions. In this scenario, the DOA parameter is a fixed value of $10°$. The tracking results under the condition of uniform acceleration of DOA are given in Figure 7. The change rate of DOA is $20°/s^2$, and the angle range is $-10$–$0°$. Figure 8 shows the tracking results under the condition of sinusoidal variation in DOA. The variation period is 1 s and the variation range is $-10$–$10°$. Figure 9 shows the tracking results under the condition of DOA step change, and the DOA step is $10°$. When there is a step change in the DOA, the tracking loop needs to converge to a new parameter. Therefore, the DOA error may increase in several loop update cycles. The DOA tracking errors in the above four scenarios are 0.053, 0.054, 0.06, and 0.11, respectively. The simulation results show that the DiLL method can adapt well to the DOA tracking problem in different dynamic scenes.

*4.3. GNSS Signal Tracking Performance Analysis*

The simulation module, which consists of three parts including the signal generation module, array signal processing module, and GNSS tracking module, was used to verify the efficacy of the algorithm. Figure 10 illustrates the simulation module. The signal generation module is used for simulating the array receiver signals. Specifically, the GNSS signal vector, interference signal vector, and noise signal vector were simulated individually, and then combined to form the received signal. On the other hand, the array signal processing module were mainly used for interference suppression, DOA estimation, and beamforming. After array weighting, the GNSS software-defined receiver [27] was used for GNSS signal tracking.
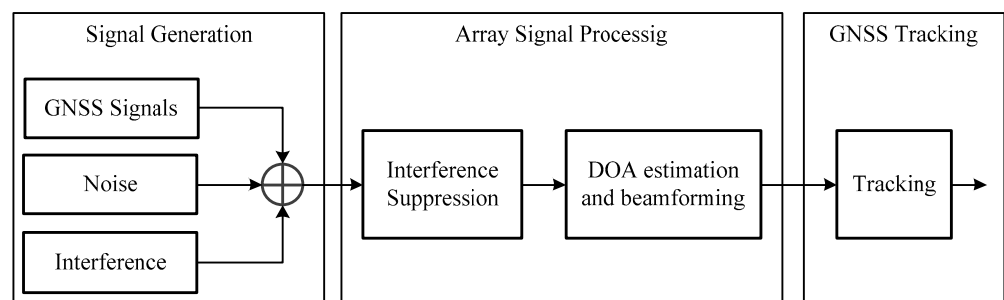


**Figure 10.** The flowchart of the simulation model.

In the simulation, one satellite navigation signal and two interference signals were simulated, a uniform line array with eight elements was used, the sampling rate was 6 MHz, and the correlation integration time was 1 ms. The navigation signal was GPS L1C/A

signal, the pseudo-code frequency was 1.023 MHz, C/N0 was 45 dBHz, and the DOA parameter was 30°. The interference signal was broadband Gaussian noise interference, the bandwidth was 2.046 MHz, the incidence direction was −40° and 55°, respectively, and the interference-to-noise-ratios were 50 dB and 55 dB, respectively. The simulation duration was 3 s, which was divided into three stages: the interference was turned off in the first second; the interference was turned on in the second second; and the C/N0 value was turned down to 30 dBHz in the third second.

In the software receiver, the performance of the proposed method was compared with the PI and MVDR methods. The PI algorithm is one of the most useful blind adaptive beamformers, and forms nulls in the direction of the jammers. The cost function of PI is as follows:

$$\min_{\mathbf{w}_{PI}} \mathbf{w}_{PI}^H \mathbf{R} \mathbf{w}_{PI} \ s.t. \ \mathbf{w}_{PI}^H \boldsymbol{\delta} = 1 \tag{23}$$

where $\boldsymbol{\delta} = [1, 0, \cdots, 0]^T$ is an $N \times 1$ vector.

The PI beamformer can be expressed as

$$\mathbf{w}_{PI} = \frac{\mathbf{R}^{-1} \boldsymbol{\delta}}{\boldsymbol{\delta}^H \mathbf{R}^{-1} \boldsymbol{\delta}} \tag{24}$$

The MVDR cost function is given as

$$\min_{\mathbf{w}_{MVDR}} \mathbf{w}_{MVDR}^H \mathbf{R} \mathbf{w}_{MVDR} \ s.t. \ \mathbf{w}_{MVDR}^H \mathbf{a}(\theta) = 1 \tag{25}$$

The solution of Equation (25) is given by

$$\mathbf{w}_{MVDR} = \frac{\mathbf{R}^{-1} \mathbf{a}(\theta)}{\mathbf{a}^H(\theta) \mathbf{R}^{-1} \mathbf{a}(\theta)} \tag{26}$$

The simulation results are shown in Figures 11–14. Figure 11 gives the normalized array pattern results of the proposed method and the PI method with and without the influence of the interference. It shows that the PI method can achieve an effective suppression of interference, but cannot achieve signal direction enhancement, and may even lead to signal energy loss. In the proposed method, the DOA parameter can be estimated accurately using DiLL, so a blind adaptive beamformer can be constructed to point the beam in the direction of the navigation signals, which can enhance the signal energy, even in the interference scenario.
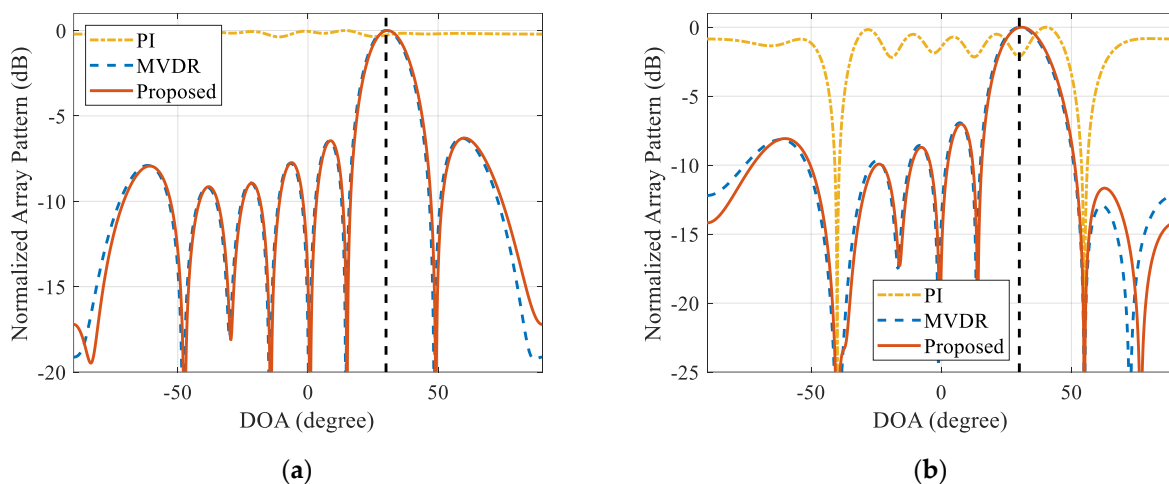


(a)                                                                        (b)

**Figure 11.** Normalized array patterns of the proposed method, the PI method, and the MVDR method: (**a**) no-interference scenario; (**b**) interference scenario.
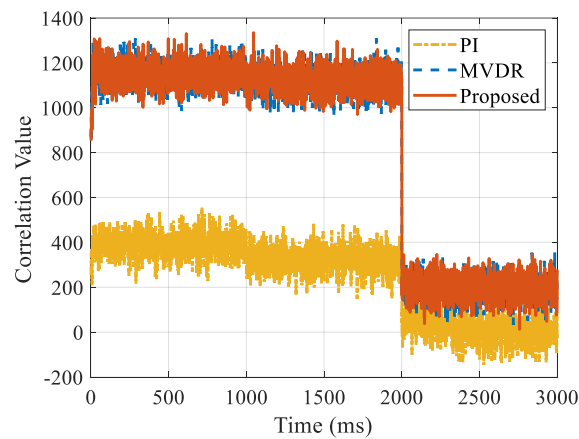
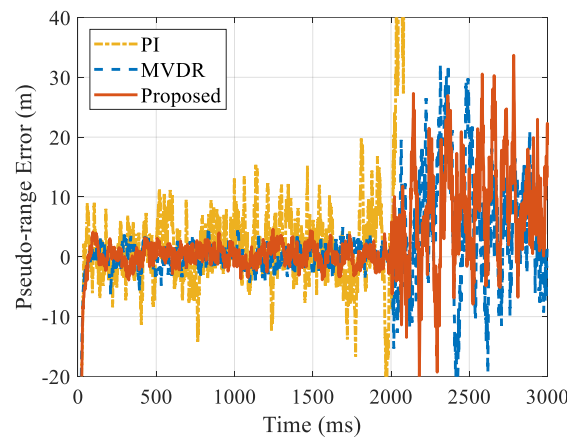**Figure 12.** The punctual branch correlation cumulative value.



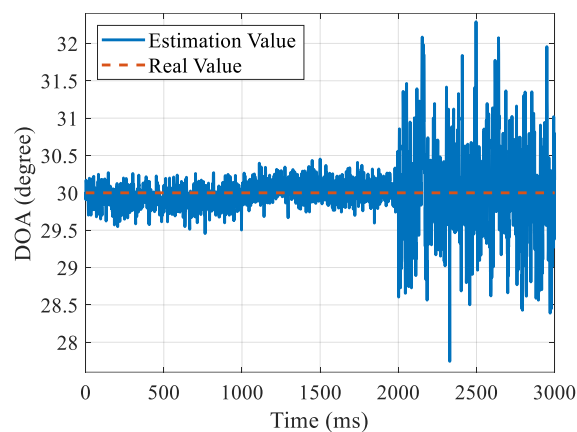**Figure 13.** Pseudo-distance measurement value.



**Figure 14.** DOA tracking results.

Figure 12 shows the punctual branch correlation value using the proposed method and the PI and MVDR methods. From the figure, it can be seen that the proposed method and MVDR can both achieve gain in the signal direction, and significantly increase signal energy compared with the PI algorithm. When the interference is turned on, the PI algorithm will cause signal energy loss while suppressing the interference as shown in Figure 12. When the C/N0 drops to 30 dBHz, the navigation signal energy after the PI algorithm is too low to cause the signal tracking loop to lose lock. However, both the proposed method and the MVDR method can still guarantee the stability tracking of the signal through the array gain,

which significantly improves the tracking performance of the navigation receiver under weak signal conditions.

Figure 13 shows the pseudo-range error calculated by the software receiver. It can be clearly seen from the figure that the accuracy of the pseudo-range measurement processed by the proposed method and the MVDR method is better than that of the PI algorithm. Under the condition of a weak signal, the PI algorithm is unable to obtain effective pseudo-range measurement due to the lock-out of the signal tracking loop, which means that the observation output of the receiver is no longer available. Although the accuracy of the pseudo-range measurement obtained by the proposed method has decreased, it can still ensure the availability of the pseudo-range measurement. The above results show that the proposed method can achieve the same performance as MVDR.

Figure 14 shows the DOA tracking results. The DOA tracking accuracy is closely related to the C/N0 value. When C/N0 is 45 dBHz, the MSE results are 0.03 degree$^2$ under no interference and 0.08 degree$^2$ under interference; when the C/N0 is 30 dBHz, the MSE value is reduced to 0.48 degree$^2$. The simulation results show that even under the condition of weak signal, high-precision DOA tracking performance can still be achieved.

## 5. Conclusions

In order to achieve interference suppression and DOA estimation, a blind adaptive beamforming algorithm for a GNSS array receiver based on DiLL is proposed. Firstly, the subspace projection principle is used to achieve interference suppression, and the direction lock loop is used to achieve high-precision tracking of the DOA of navigation signals in the correlation domain. Then, the beamformer is constructed with the estimated DOA estimation results, which can provide gain by forming a beam in the satellite direction. After the array signals are weighted, interference suppression and navigation signal enhancement can be realized. The proposed method can realize DOA estimation in the presence of interference with low computational complexity, and thus achieve stable DOA tracking in dynamic scenes. It deserves great attention in the field of GNSS array antenna receivers.

**Author Contributions:** J.W. performed the theoretical study, conducted the experiments, processed the data, and wrote the manuscript. X.T. and L.H. provided research suggestions and revised the manuscript. S.N. helped in performing the experiments. F.W. provided the experimental equipment and suggestions for the manuscript. All authors have read and agreed to the published version of the manuscript.

**Data Availability Statement:** No date supporting.

**Conflicts of Interest:** The authors declare no conflict of interest.

## References

1. Liu, J.; Gao, K.; Guo, W.; Cui, J.; Guo, C. Role, path, and vision of "5G + BDS/GNSS". *Satell. Navig.* **2020**, *1*, 23. [CrossRef]
2. Elghamrawy, H.; Karaim, M.; Korenberg, M.; Noureldin, A. High-Resolution Spectral Estimation for Continuous Wave Jamming Mitigation of GNSS Signals in Autonomous Vehicles. *IEEE Trans. Intell. Transp. Syst.* **2021**, *23*, 7881–7895. [CrossRef]
3. Lu, Z.; Song, J.; Huang, L.; Ren, C.; Xiao, Z.; Li, B. Distortionless 1/2 Overlap Windowing in Frequency Domain Anti-Jamming of Satellite Navigation Receivers. *Remote Sens.* **2022**, *14*, 1801. [CrossRef]
4. Chaparro, D.; Feldman, A.F.; Chaubell, M.J.; Yueh, S.H.; Entekhabi, D. Robustness of Vegetation Optical Depth Retrievals Based on L-Band Global Radiometry. *IEEE Trans. Geosci. Remote Sens.* **2022**, *60*, 4413417. [CrossRef]
5. Sun, Y.; Chen, F.; Lu, Z.; Wang, F. Anti-Jamming Method and Implementation for GNSS Receiver Based on Array Antenna Rotation. *Remote Sens.* **2022**, *14*, 4774. [CrossRef]
6. Wolfley, O.; Schvartzman, D.; Mansur, B.; Fusselman, J.D.; Zhang, Y.R.; Snelling, B. Three-dimensional anti-jamming array processing for GNSS-based navigational aid inspection. In Proceedings of the Radar Sensor Technology XXVI 2022, Virtual, 6–12 June 2022; The Society of Photo-Optical Instrumentation Engineers (SPIE): Bellingham, DC, USA, 2022.

7.  Compton, R.T., Jr. The Power-Inversion Adaptive Array: Concept and Performance. *IEEE Trans. Aerosp. Electron. Syst.* **1979**, *AES-15*, 803–814. [CrossRef]
8.  Yang, X.; Liu, W.; Chen, F.; Lu, Z.; Wang, F. Analysis of the Effects Power-Inversion (PI) Adaptive Algorithm Have on GNSS Received Pseudorange Measurement. *IEEE Access* **2019**, *10*, 70242–70251. [CrossRef]
9.  Lu, Z.; Nie, J.; Wan, Y.; Ou, G. Optimal reference element for interference suppression in GNSS antenna arrays under channel mismatch. *IET Radar Sonar Navig.* **2017**, *11*, 1161–1169. [CrossRef]
10. Fernandez-Prades, C.; Arribas, J.; Closas, P. Robust GNSS Receivers by Array Signal Processing: Theory and Implementation. *Proc. IEEE* **2016**, *104*, 1207–1220. [CrossRef]
11. Dai, X.; Nie, J.; Chen, F.; Ou, G. Distortionless space-time adaptive processor based on MVDR beamformer for GNSS receiver. *IET Radar Sonar Navig.* **2017**, *11*, 1488–1494. [CrossRef]
12. Jia, Q.; Wu, R.; Wang, W.; Lu, D.; Wang, L. Adaptive blind anti-jamming algorithm using acquisition information to reduce the carrier phase bias. *GPS Solut.* **2018**, *22*, 99. [CrossRef]
13. Wu, J.; Huang, L.; Tang, X.; Li, B.; Wang, F. Distortionless Blind Beamformer for Interference Suppression in GNSS Antenna Array Receiver. In Proceedings of the 11th China Satellite Navigation Conference, CSNC 2020, Chengdu, China, 22–25 November 2020; Springer Science and Business Media Deutschland GmbH: Berlin, Germany, 2020; Volume 652, pp. 733–741.
14. Tan, J.; Nie, Z.; Peng, S. Quadratic forward/backward spatial smoothing polarization smoothing MUSIC algorithm for low angle estimation. In Proceedings of the 2019 IEEE Radar Conference, RadarConf 2019, Boston, MA, USA, 22–26 April 2019; Institute of Electrical and Electronics Engineers Inc.: Piscateville, NJ, USA, 2019.
15. Zhang, W.; Han, Y.; Jin, M.; Li, X.-S. An Improved ESPRIT-Like Algorithm for Coherent Signals DOA Estimation. *IEEE Commun. Lett.* **2019**, *24*, 339–343. [CrossRef]
16. Chen, X.; Morton, Y. Iterative subspace alternating projection method for GNSS multipath DOA estimation. *IET Radar Sonar Navig.* **2016**, *10*, 1260–1269. [CrossRef]
17. Weiland, L.; Wiese, T.; Utschick, W. Multipath mitigation using OMP and Newton's method for multi-antenna GNSS receivers. In Proceedings of the 7th IEEE International Workshop on Computational Advances in Multi-Sensor Adaptive Processing, CAMSAP 2017, Curacao, The Netherlands, 10–13 December 2017; Institute of Electrical and Electronics Engineers Inc.: Piscateville, NJ, USA, 2017; pp. 1–5.
18. Rao, C.; Sastry, C.; Zhou, B. Tracking the direction of arrival of multiple moving targets. *IEEE Trans. Signal Process.* **1994**, *42*, 1133–1144. [CrossRef]
19. Denic, N.; Dimitrijevic, B.; Miloevic, N.; Nikolic, Z. Three dimensional direction lock loop for DS/CDMA systems. In Proceedings of the TELSIKS 2007-8th International Conference on Telecommunications in Modern Satellite, Cable and Broadcasting Services, Nis, Serbia, 26–28 September 2007; IEEE Computer Society: Washington, DC, USA, 2007; pp. 11–14.
20. Min, S.; Seo, D.; Lee, K.B.; Kwon, H.; Lee, Y.-H. Direction-of-Arrival Tracking Scheme for DS/CDMA Systems: Direction Lock Loop. *IEEE Trans. Wirel. Commun.* **2004**, *3*, 191–202. [CrossRef]
21. Walid, G.D.; Hassan, M.E. DOA tracking in multipath environment based on the Direction Lock Loop. In Proceedings of the 2007 IEEE International Conference on Signal Processing and Communications, ICSPC 2007, Dubai, United Arab Emirates, 24–27 November 27; IEEE Computer Society: Washington, DC, USA, 2007; pp. 1099–1102.
22. Wang, B.; Shivaramaiah, N.C.; Akos, D.M.; Wei, J. GNSS direction of arrival tracking using the rotate-to-zero direction lock loop. *GPS Solut.* **2020**, *24*, 39. [CrossRef]
23. Cheng, X.-Z.; Zhu, D.-R.; Zhang, S.; He, P. Tracking Positioning Algorithm for Direction of Arrival Based on Direction Lock Loop. *Futur. Internet* **2015**, *7*, 214–224. [CrossRef]
24. Guan, G.; Xian, D.; Zhang, K.; Gao, Y.; Zhu, X. Direction-of-arrival (DOA) tracking using improved direction lock loop with real-time bias correction for antenna array based GNSS receivers. *Adv. Space Res.* **2017**, *60*, 2733–2741. [CrossRef]
25. Yang, B.; Cui, W.; Liu, Y.; Gao, B.; Mei, F.; Xu, H. DOA tracking using an improved direction lock loop based on a three-element L-shaped array. *GPS Solut.* **2022**, *26*, 108. [CrossRef]
26. Sgammini, M.; Antreich, F.; Kurz, L.; Michael, M.; Tobias, G. Blind adaptive beamformer based on orthogonal projections for GNSS. In Proceedings of the ION ITM 2012, Nashville, TN, USA, 17–21 September 2012; Institute of Navigation: Manassas, VA, USA, 2012; pp. 926–935.
27. Kai, B.; Akos, D.M.; Bertelsen, N.; Rinder, P.; Jensen, S.H. *A Softwaredefined GPS and Galileo Receiver: A Single-Frequency Approach*; Springer: New York, NY, USA, 2007.